

Spinelectronic investigation of the quaternary vanadium fluoride Rb_2NaVF_6 : Ab-initio method

M. Berber^{a,b,*}, B. Nour Bouzouira^{a,c}, H. Abid^d, A. Boudali^e, and H. Moujri^f

^aCentre Universitaire Nour Bachir El Bayadh, 32000 El Bayadh, Algérie,

^bLaboratoire d'Instrumentation et Matériaux Avancés,

Centre Universitaire Nour Bachir, El-Bayadh, BP 900 route Aflou, 32000, Algérie,

^cLaboratory of Physical Chemistry of Advanced Materials, University of Djillali Liabes, BP 89, Sidi-Bel-Abbes 22000, Algeria.

^dApplied Materials Laboratory, Research Center,

Sidi Bel Abbés Djillali Liabes University, 22000, Algeria.

^eLaboratory of Physico-Chemical Studies, University of Saida, 20000 Saida, Algeria.

^fRenewable Energy Laboratory and dynamic systems,

Faculté des Sciences Ain-Chock, Université Hassan II de Casablanca, Morocco.

Received 11 May 2020; accepted 8 June 2020

In this study, we have investigated the structural, electronic, and magnetic properties of the Rb_2NaVF_6 compound. We have performed our calculations by the use of first-principle methods based on spin-polarized density functional theory, where the electronic exchange-correlation potential is treated by the generalized gradient approximation GGA-PBESol coupled with the improved TB-mBJ approach. The calculated structural parameters of Rb_2NaVF_6 are in good agreement with the available experimental data. Rb_2NaVF_6 exhibits a half-metallic ferromagnetic feature with a spin polarization of 100% at the Fermi level and a direct large half-metallic gap of 3.582 eV. The total magnetic moments are 2 μB . This material is half-metallic ferromagnets, and it can be potential candidates for spintronics applications at a higher temperature.

Keywords: DFT; TB-mBJ; electronic structures; half-metallic ferromagnetic.

PACS: 71.15.Mb; 71.20.-b; 74.25.Ha

DOI: <https://doi.org/10.31349/RevMexFis.66.604>

1. Introduction

Spintronics is the investigation of the fundamental spin of the electron and its combined magnetic moment, adding to its essential electronic charge, in solid-state devices [1]. Furthermore, to charge state, electron spins are used as a further degree of freedom, with employment in the performance of data storage and transfer. Spintronic devices are almost frequently synthesized in dilute magnetic semiconductors (DMS), Perovskite, and Heusler alloys and are of exceptional attraction in the field of quantum computing and neuromorphic computing [2]. Spintronics is a field of study in which, researchers are looking for materials to ameliorate the accomplishment of their electronic and magnetic properties and get a large half-ferromagnetic (HM) gap (G_{HM}). The HM *i.e.*, spin-flip excitation, gap is identified to be the least possible energy with respect to the Fermi level of the majority (minority) spin between the minimal energy of the conduction bands and the absolute value of maximum energy of the valence bands [3,4]. Last decade, several experimental and theoretical research have been developed for this purpose. Recently, multiple works have treated the magnetic properties of the binary semiconductor III-V and II-VI doped by transition elements, Mn-doped InSb [5], Cr doped InSb [6], V doped GaP [7], Co-doped ZnS and (Al, Co) co-doped [8], and Mn-doped ZnO [9]. Shabir *et al.* studied the double perovskites system Ba_2CoUO_6 and report half-metallic comportment, with

a half-metallic gap $G_{HM} = 1.98$ eV [10]. A. Rafi *et al.* studied the perovskite selenide and tellurite compounds CoSeO_3 , CoTeO_3 , NiSeO_3 , and NiTeO_3 [11]. The half-Heusler Alloy MgCaB has been investigated by A. Abada [12], with a value of G_{HM} of about 0.305 eV.

This aim of this work is to predict the structural, electronic, and half-metallic ferromagnetic properties of quaternary vanadium fluoride Rb_2NaVF_6 . We have used in our calculation the generalized gradient approximation functional (GGA-PBESol) [13] and Becke-Johnson exchange potential [14] with Tran-Blaha modified Becke-Johnson (TB-mBJ) potential [15] based on full-potential linearized augmented plane-wave (FP-LAPW) method within first-principle approaches of spin-polarized density functional theory (SP-DFT) [16]. This article is redacted as follows: In Sec. 2, we describe the method of the calculation. In Sec. 3, we demonstrate the details of the collected results and discuss the structural, electronic, and magnetic properties of the Rb_2NaVF_6 compound. Section 4 summarizes the key findings of our current research.

2. Computational method

In this study, we have utilized the FP-LAPW method based on SP-DFT [16] as realized in the WIEN2K software [17,18] to predict the structural, electronic, and magnetic properties

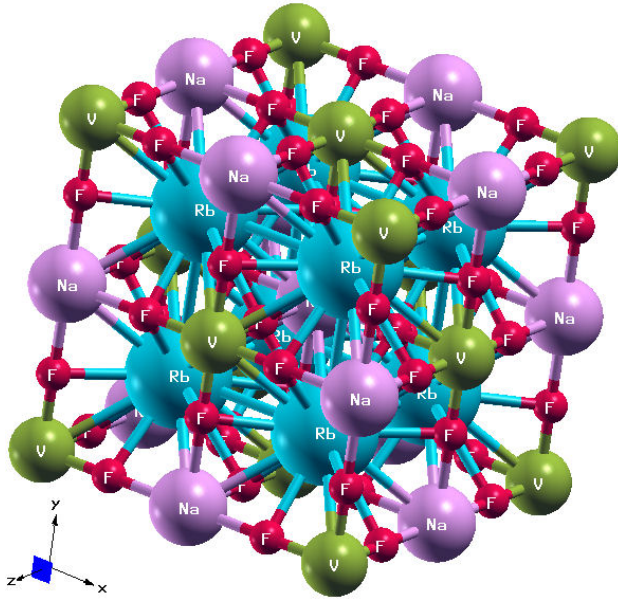


FIGURE 1. Crystal structure of quaternary vanadium fluoride Rb_2NaVF_6 .

of quaternary vanadium fluoride Rb_2NaVF_6 . The structural properties are predicted by applying the GGA-PBEsol [13], while the electronic structures and magnetic properties are calculated with GGA-PBEsol along with TB-mBJ exchange potential. In this study, we have chosen the following calculation parameters: the $K_{\text{max}} = 9 (\text{RMT})^{-1}$ (K_{max} is the plane wave cut-off, and RMT is the smallest of all atomic sphere radii). The Fourier expanded charge density was limited at $G_{\text{max}} = 12 (\text{Ryd})^{1/2}$, the l -expansion of the non-spherical potential and charge density was performed up to $l_{\text{max}} = 10$. The cut-off energy is set to -7 Ryd to separate the core from valence states. The muffin-tin radii (MT) for Rb, Na, V and F to be 2.50, 1.98, 1.78 and 1.69 atomic units (a.u.), respectively. The iteration process is repeated until the calculated total energy and charge of the crystal converge to less than 0.0001 Ryd and 0.001e, respectively.

3. Results and discussion

3.1. Stability and structural properties

In 1966, R. Hoppe studied the crystallography of the compound Rb_2NaVF_6 [19,20]. The quaternary vanadium fluo-

TABLE I. Rb, Na, V and F atoms positions.

Atoms		Position		
		X	Y	Z
Rb	Atom 1	0.250	0.250	0.250
	Atom 2	0.750	0.750	0.750
Na	Atom 1	0.500	0.500	0.500
V	Atom 1	0.000	0.000	0.000
	Atom 2	0.770	0.000	0.000
F	Atom 1	0.230	0.000	0.000
	Atom 2	0.770	0.000	0.000
	Atom 3	0.000	0.230	0.000
	Atom 4	0.000	0.770	0.000
F	Atom 5	0.000	0.000	0.230
	Atom 6	0.000	0.000	0.770

ride Rb_2NaVF_6 crystallizes in the cubic NaCl (B1) structure with a space group of $(\text{Fm}\bar{3}\text{m})$ (no. 225). Figure 1 and Table I exhibit the crystal structure and the Rb, Na, V, and F atoms positions of Rb_2NaVF_6 , respectively. We have optimized the Rb_2NaVF_6 , with and without spin-polarized calculations. We have computed the total energies corresponding to the unit cell volumes and fitted to the Birch-Murnaghan's equation of state (EOS) [21] to verify the phase stability of the compound. And evaluate the structural properties such as the equilibrium lattice constant a , bulk modulus B and the

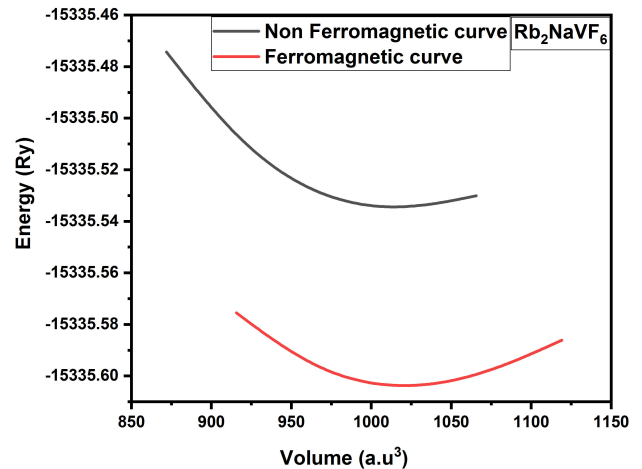


FIGURE 2. Volume optimization curve of quaternary vanadium fluoride Rb_2NaVF_6 .

TABLE II. Calculated lattice constant (a), bulk modulus (B), pressure derivative B' , minimum equilibrium energy E_0 , and equilibrium volume V_0 of Rb_2NaVF_6 .

a (Å)	B (GPa)	B'	Energy E_0 (Ry)	Volume V_0 (a.u. ³)	character
8.4499, 8.46 [19,20]	69.4580	5.2094	-15335.605695	1017.8553	Ferromagnetic
8.4339, 8.46 [19,20]	70.7549	4.6757	-15335.536252	1012.1034	Non-magnetic

bulk modulus pressure derivative B' , the inspected structural constants of Rb_2NaVF_6 are recapitulated in Table II, our results are in good agreement with the obtainable theoretical and experimental data. By comparing the two curves, it is obvious that the ferromagnetic curve is below the non-magnetic curve, which indicates that the Rb_2NaVF_6 structure is stable in ferromagnetic phase. The energy versus volume curves are shown in the Fig. 2.

3.2. Electronic, magnetic properties and half-metallic compartment

In this section, we have predicted the electronic band structure, total (TDOS), and partial (PDOD) densities of states for Rb_2NaVF_6 , using GGA-PBEsol [13] accompanying with (TB-mBJ) of Tran-Blaha modified Becke-Johnson approximation [14,22]. Figures 3 and 4 exhibit the band structure of Rb_2NaVF_6 for spin-up and spin-down, respectively. It is apparent in Fig. 3 that the highest valence band is above the Fermi level, hence the metallic behavior of the structure. For Fig. 4, we mark two gaps, the half-metallic ferromagnetic

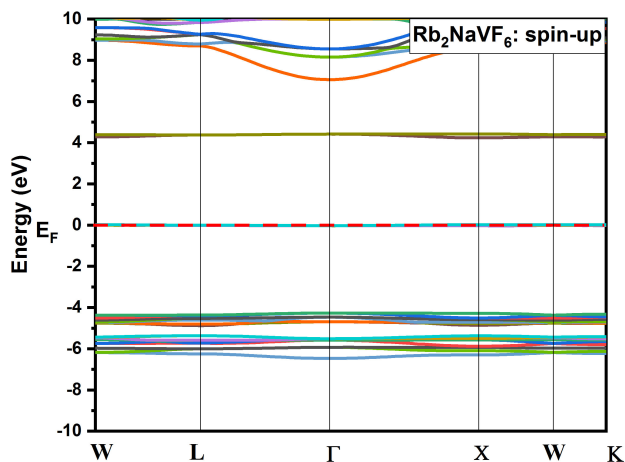


FIGURE 3. Spin-up band structure obtained with TB-mBJ for Rb_2NaVF_6 .

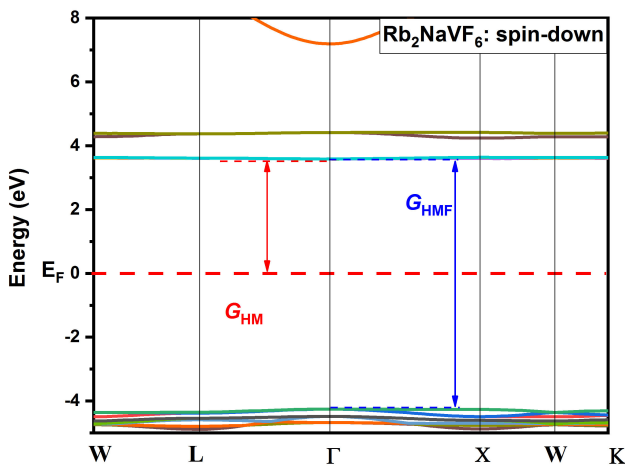


FIGURE 4. Spin-down band structure obtained with TB-mBJ for Rb_2NaVF_6 .

gap (G_{HMF}) and the half-metallic gap (G_{HM}), G_{HMF} is the energy difference between the valence-band maximum (VBM) and conduction-band minimum (C_{BM}) [4]. Rb_2NaVF_6 compound has a direct half-metallic ferromagnetic gap at $\Gamma - \Gamma$ of 7.837 eV and large half-metallic gap at $\Gamma - \Gamma$ high-symmetry point of 3.582 eV. The non-zero values of the half-metallic gap for Rb_2NaVF_6 demonstrate it to be true half-metallic ferromagnets and making it promising materials for employment in spintronic applications.

To know the origin of the ferromagnetic and the half-metallic behavior, we have calculated the densities of states (DOS) around the Fermi level (E_F). Fig. 5 shows the total densities of states of Rb_2NaVF_6 , Rb, Na, V, and F atoms. We notice that the total density of states (TDOS) is symmetrical

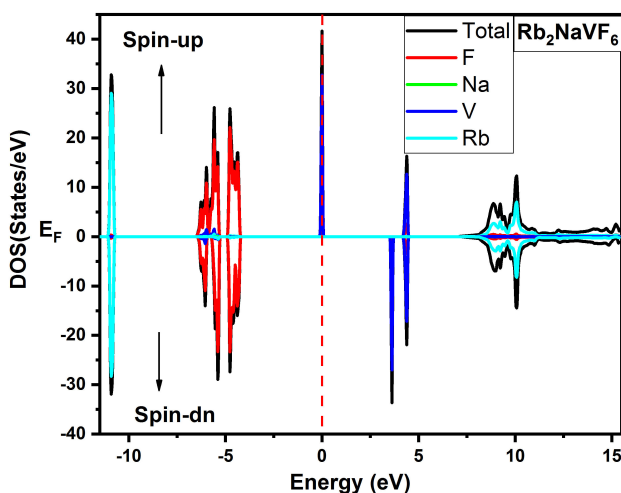


FIGURE 5. Spin-polarized total densities of states (TDOS) of Rb_2NaVF_6 . The Fermi level is set to zero. (vertical dotted red line).

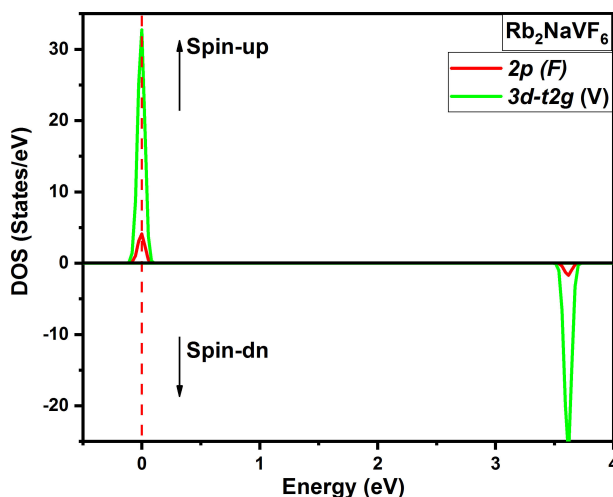


FIGURE 6. Spin-polarized partial densities of states (PDOS) of Rb_2NaVF_6 . The Fermi level is set to zero. (vertical dotted red line)

TABLE III. Calculated total and local magnetic moments of the relevant Rb, Na, V, and F atoms and in the interstitial sites (in Bohr magneton μ_B) for Rb₂NaVF₆.

Compound	Total (μ_B)	Rb (μ_B)	Na (μ_B)	V (μ_B)	F (μ_B)	Interstitial (μ_B)
Rb ₂ NaVF ₆	2.00001	0.00018	0.00009	1.71792	0.00495	0.25194

TABLE IV. Calculated $p-d$ exchange splitting $\Delta_x^v(pd) = E_v^\downarrow - E_v^\uparrow$ and $\Delta_x^c(pd) = E_c^\downarrow - E_c^\uparrow$, and exchange constants $N_0\alpha$ and $N_0\beta$ for Rb₂NaVF₆.

Compound	$\Delta_x^c(pd)$ (eV)	$\Delta_x^v(pd)$ (eV)	$N_0\alpha$	$N_0\beta$
Rb ₂ NaVF ₆	3.584	0.013	41.724	0.151

except at Fermi level (0 eV) for spin-up and 3.618 eV for spin-down. The total densities of states are dominated by Rb between the energy from -11.102 and -10.694 eV, and at energy more than 8 eV. While the F dominates at an energy between -6.476 and -4.190 eV. Moreover, V dominates the peaks, which are at the energies 0, 3.618, and 4.380 eV. The half-metallic nature can be seen in the channel spin-down. To comprehend the source of the half-metallic gap and the half-metallic ferromagnetic gap we have plotted the partial densities of states. Figure 6 represent the partial densities of states of Rb₂NaVF₆, the pike located at the 0 eV (Fermi level) and 3.618 eV are mainly formed by the $3d-t2g$ (V) and $2p$ (F) states. The TDOS of Rb₂NaVF₆ depicted asymmetrical states of spin-up and spin-down due to strong $p-d$ hybridization between the $2p$ (O) and $3d-t2g$ (V) states around the Fermi level for the majority-spin direction. This hybridization occurs mainly at the top of the majority-spin valence bands and crosses the Fermi level, leading to the metallic nature for Rb₂NaVF₆ compounds, with spin polarization of 100% by using the following expression [23]:

$$p = \frac{N \uparrow (E_F) - N \downarrow (E_F)}{N \uparrow (E_F) + N \downarrow (E_F)} \times 100\%, \quad (1)$$

where P is the spin polarization, $N \uparrow (E_F)$ and $N \downarrow (E_F)$ are the densities of states of the majority spin and minority spin around the Fermi level, respectively. Table III display the total and local magnetic moments of Rb₂NaVF₆. To interpret the implications of the $p-d$ interchange phenomenon on the magnetic behavior, we have calculated the total and local magnetic moments of the Rb, Na, V, and F atoms as well as the interstitial sites. The results exhibit the total magnetic moment for the Rb₂NaVF₆ compound was around 2 μ_B , usually caused by the V atoms' the local magnetic moment. $3d$ (V) majority-spin states, which are partially occupied with three electrons, resulting in a total magnetic moment of 2 μ_B . Otherwise, the calculated magnetic moment of the V atom is reduced to 1.71792 μ_B and minor local magnetic moments are induced at Rb, Na, F, and interstitial sites overdue to the $p-d$ exchange interaction between $2p$ (F) and $3d-t2g$ (V) states. Important parameters established on band structures such as $p-d$ exchange splitting have also been calculated, $\Delta_x^c(pd) = E_c^\downarrow - E_c^\uparrow$ and $\Delta_x^v(pd) = E_v^\downarrow - E_v^\uparrow$ and the $s-d$

exchange constants $N_0\alpha$ (conduction band) and the $p-d$ exchange constant $N_0\beta$ (valence band).

Both $N_0\alpha$ and $N_0\beta$ parameters are calculated employing the mean-field theory whose expression is as follows [24,25]:

$$N_0\alpha = \frac{\Delta E_c}{x \langle s \rangle}, \quad (2)$$

$$N_0\beta = \frac{\Delta E_v}{x \langle s \rangle}, \quad (3)$$

where $\Delta E_c = E_c^\downarrow - E_c^\uparrow$ is the conduction band-edge spin-splitting and $\Delta E_v = E_v^\downarrow - E_v^\uparrow$ is the valence band-edge spin-splitting of Rb₂NaVF₆ at high symmetry point Γ . $\langle s \rangle$ is the half total magnetic moment per vanadium atom and x is the concentration of V in the structure. Table IV exhibits the calculated $p-d$ exchange splitting and exchange parameters. The positive $N_0\alpha$ constant indicates the ferromagnetic coupling between the $3d$ states of V and conduction bands. Also, we have calculated an important property of spin-polarized materials, the $\Delta_x^v(pd)$ and $\Delta_x^c(pd)$ parameters, which determines the attraction character in the Rb₂NaVF₆. However, the positivity $\Delta_x^v(pd)$ of Rb₂NaVF₆ structure means that the potential of minority spin is effective compared to the majority spin [26,27].

4. Conclusion

We have theoretically calculated the structural, electronic, and magnetic properties of the cubic Rb₂NaVF₆ system, using the density functional theory and it is concluded that:

- The lattice constant is in good agreement with the obtainable experimental data.
- Rb₂NaVF₆ is metallic for the majority spin states while semiconducting for the minority spin state with a direct large half-metallic gap of 3.582 eV.
- Rb₂NaVF₆ exhibits 100% spin polarization at the Fermi level (EF).
- The Rb₂NaVF₆ compound can be used in spintronic applications and can operate at a higher temperature due to its half-metallic properties and with a wide bandgap.

1. S. A. Wolf *et al.*, Spintronics: A Spin-Based Electronics Vision for the Future, *Science* **294** (2001) 1488, <https://doi.org/10.1126/science.1065389>.
2. S. Umesh and S. Mittal, A survey of spintronic architectures for processing-in-memory and neural networks, *J. Syst. Archit.* **97** (2019) 349, <https://doi.org/10.1016/j.sysarc.2018.11.005>.
3. K. L. Yao, G. Y. Gao, Z. L. Liu and L. Zhu, Half-metallic ferromagnetism of zinc-blende CrS and CrP: a first-principles pseudopotential study, *Solid State Commun.* **133** (2005) 301, <https://doi.org/10.1016/j.ssc.2004.11.016>.
4. G. Y. Gao *et al.*, Half-metallic ferromagnetism in zinc blende CaC, SrC, and BaC from first principles, *Phys. Rev. B* **75** (2007) 174442, <https://doi.org/10.1103/PhysRevB.75.174442>.
5. A. Laroussi *et al.*, First-Principles Calculations of the Structural, Electronic and Magnetic Properties of Mn-Doped InSb by Using mBJ Approximation for Spintronic Application, *Acta Phys. Pol. A* **135** (2019) 451, <https://doi.org/10.12693/APhysPolA.135.451>.
6. A. Laroussi *et al.*, The effect of substitution of Cr impurities at the In sites on the structural, electronic and magnetic properties of InSb: a DFT study within mBJ potential, *Appl. Phys. A* **125** (2019) 676, <https://doi.org/10.1007/s00339-019-2973-2>.
7. M. E. A. Monir *et al.*, Density functional theory investigation of half-metallic ferromagnetism in V-doped GaP alloys, *J. Magn. Mater.* **497** (2020) 166067, <https://doi.org/10.1016/j.jmmm.2019.166067>.
Q50:
8. M. S. Khan, L. Shi, B. Zou, and S. Ali, Theoretical investigation of optoelectronic and magnetic properties of Co-doped ZnS and (Al,Co) co-doped ZnS, *Comput. Mater. Sci.* **174** (2020) 109491, <https://doi.org/10.1016/j.commatsci.2019.109491>.
9. J. Marquina, E. Quintero, F. Ruetter, and Y. Bentarcut, Theoretical study of Mn doping effects and O or Zn vacancies on the magnetic properties in wurtzite ZnO, *Chin. J. Phys.* **63** (2020) 63, <https://doi.org/10.1016/j.cjph.2019.09.037>.
10. S. A. Mir and D. C. Gupta, Exploration of uranium double perovskites Ba₂MUO₆ (M=Co, Ni) for magnetism, spintronic and thermoelectric applications, *J. Magn. Mater.* **493** (2020) 165722, <https://doi.org/10.1016/j.jmmm.2019.165722>.
11. A. R. M. Iasir *et al.*, Electronic and magnetic properties of perovskite selenite and tellurite compounds: CoSeO₃, NiSeO₃, CoTeO₃, and NiTeO₃, *Phys. Rev. B* **101** (2020) 045107, <https://doi.org/10.1103/PhysRevB.101.045107>.
12. A. Abada and N. Marbouh, Study of New d⁰ Half-Metallic Half-Heusler Alloy MgCaB: First-Principles Calculations, *J. Supercond. Nov. Magn.* **33** (2020) 889, <https://doi.org/10.1007/s10948-019-05288-1>.
13. J. P. Perdew, K. Burke, and M. Ernzerhof, Generalized Gradient Approximation Made Simple, *Phys. Rev. Lett.* **77** (1996) 3865, <https://doi.org/10.1103/PhysRevLett.77.3865>.
14. (Are the authors referring to A. D. Becke and E. R. Johnson, A simple effective potential for exchange, *J. Chem. Phys.* **124** (2006) 221101, <https://doi.org/10.1063/1.2213970>).
15. F. Tran and P. Blaha, Accurate Band Gaps of Semiconductors and Insulators with a Semilocal Exchange-Correlation Potential, *Phys. Rev. Lett.* **102** (2009) 226401, <https://doi.org/10.1103/PhysRevLett.102.226401>.
16. W. Kohn and L. J. Sham, Self-Consistent Equations Including Exchange and Correlation Effects, *Phys. Rev.* **140** (1965) A1133, <https://doi.org/10.1103/PhysRev.140.A1133>.
17. K. Schwarz, P. Blaha, and G. K. H. Madsen, Electronic structure calculations of solids using the WIEN2k package for material sciences, *Comput. Phys. Commun.* **147** (2002) 71, [https://doi.org/10.1016/S0010-4655\(02\)00206-0](https://doi.org/10.1016/S0010-4655(02)00206-0)
18. P. Blaha *et al.*, WIEN2k: An APW+lo program for calculating the properties of solids, *J. Chem. Phys.* **ESS2020** (2020) 074101, <https://doi.org/10.1063/1.5143061@jcp.2020.ESS2020.issue-1>.
19. R. Hoppe, Madelung Constants, *Angew. Chemie Int. Ed. Engl.* **5** (1966) 95, <https://doi.org/10.1002/anie.196600951>.
20. E. Alter and R. Hoppe, Über Hexafluorovanadate(III). Cs₂MVF₆ und Rb₂MVF₆ (M=Ti, K und Na); mit einer Bemerkung über Na₃VF₆, *Z. Anorg. Allg. Chemie* **412** (1975) 110, <https://doi.org/10.1002/zaac.19754120203>.
21. F. Birch, Finite Elastic Strain of Cubic Crystals, *Phys. Rev.* **71** (1947) 809, <https://doi.org/10.1103/PhysRev.71.809>.
22. F. Tran, P. Blaha, and K. Schwarz, Band gap calculations with Becke-Johnson exchange potential, *J. Phys. Condens. Matter* **19** (2007) 196208, <https://doi.org/10.1088/0953-8984/19/19/196208>.
23. J. Bai *et al.*, The effects of alloying element Co on Ni-Mn-Ga ferromagnetic shape memory alloys from first-principles calculations, *Appl. Phys. Lett.* **98** (2011) 164103, <https://doi.org/10.1063/1.3582239>.
24. S. Sanvito, P. Ordejón, and N. A. Hill, First-principles study of the origin and nature of ferromagnetism in Ga_{1-x}Mn_xAs, *Phys. Rev. B* **63** (2001) 165206, <https://doi.org/10.1103/PhysRevB.63.165206>.

25. H. Raebiger, A. Ayuela, and R. M. Nieminen, Intrinsic hole localization mechanism in magnetic semiconductors, *J. Phys. Condens. Matter* **16** (2004) L457, <https://doi.org/10.1088/0953-8984/16/41/L05>.
26. U. P. Verma, S. Sharma, N. Devi, P. S. Bisht, and P. Rajaram, Spin-polarized structural, electronic and magnetic properties of diluted magnetic semiconductors $\text{Cd}_{1-x}\text{Mn}_x\text{Te}$ in zinc blende phase, *J. Magn. Magn. Mater.* **323** (2011) 394, <https://doi.org/10.1016/j.jmmm.2010.09.016>.
27. V. L. Moruzzi, J. F. Janak, and A. R. Williams, *Calculated electronic properties of metals* (Elsevier, Amsterdam, 2013), <https://doi.org/10.1016/C2013-0-03017-4>.